Electronic Supplementary Information (ESI)

Cu-NHC based phosphorescent binuclear Iridium(III)/Copper(I) complex with an unpredictable near-linear two-coordination mode

Chao Shi,[a b] Manli Huang,[c] Qiuxia Li,[a] Guohua Xie,[c] Chuluo Yang*[c] and Aihua Yuan*[a b]

Contents:

Synthesis

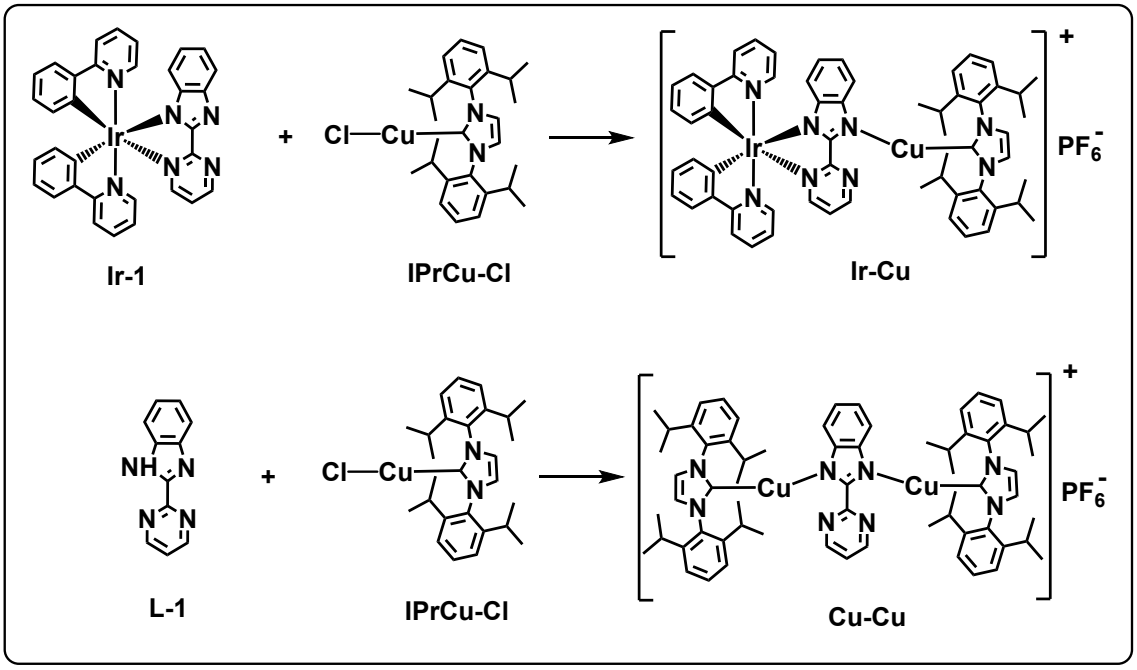

Fig. S1. The synthetic routes for binuclear Iridium(III)/Copper(I) complex **Ir-Cu** and Copper(I)/Copper(I) complex **Cu-Cu**.

X-ray crystal structure analysis

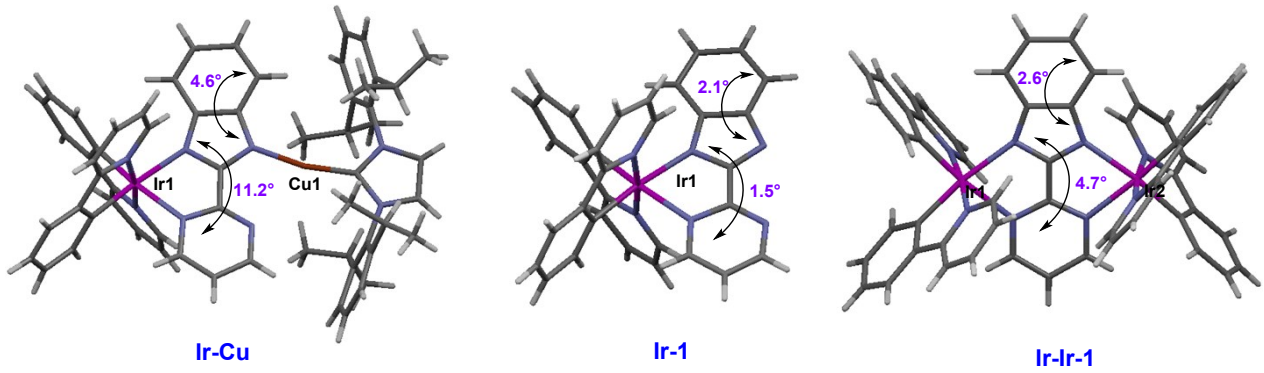

Fig. S2. The dihedral angles comparisons for ligand **L-1** in complex **Ir-Cu**, **Ir-1** and **Ir-Ir-1**.

Table S1. Crystallographic Data for **Ir-Cu**

Complex	**Ir-Cu**
chemical formula	$C_{60}H_{59}CuIrN_8F_6P$
formula weight	1292.86
crystal size (mm)	0.18 ×0.21 × 0.23
temperature (K)	291
radiation	0.71073
crystal system	Triclinic
space group	P-1
a(Å)	13.565(2)
b(Å)	14.327(2)
c(Å)	17.823(2)
α(°)	70.405(3)
β(°)	69.494(2)
γ(°)	62.654(2)
V(Å^3)	2817.7(7)
Z	2
$\rho_{(calc)}$ (g/cm^3)	1.524

F (000)	1300
absorp.coeff. (mm^{-1})	2.831
θ range (deg)	1.6 to 27.7
reflns collected	56406 (R_{int} = 0.040)
indep. reflns	13006
Refns obs.[$I > 2\sigma(I)$]	9742
data/restr/paras	13006/0/701
GOF	1.04
R_1/wR_2 [$I > 2\sigma(I)$]	0.0549/0.0808
R_1/wR_2 (all data)	0.0838/0.0864
larg peak and hole(e/Å^3)	2.31/–1.21

Photophysical properties

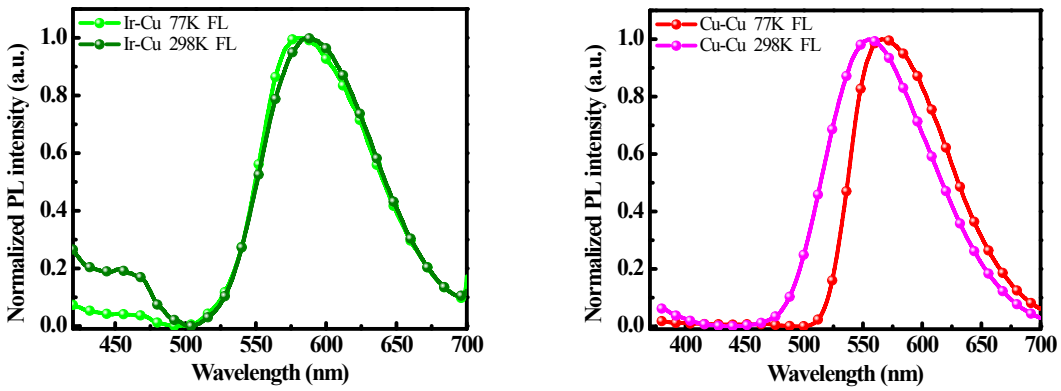

Fig. S3. PL spectrum comparison for **Ir-Cu** and **Cu-Cu** at different temperatures.

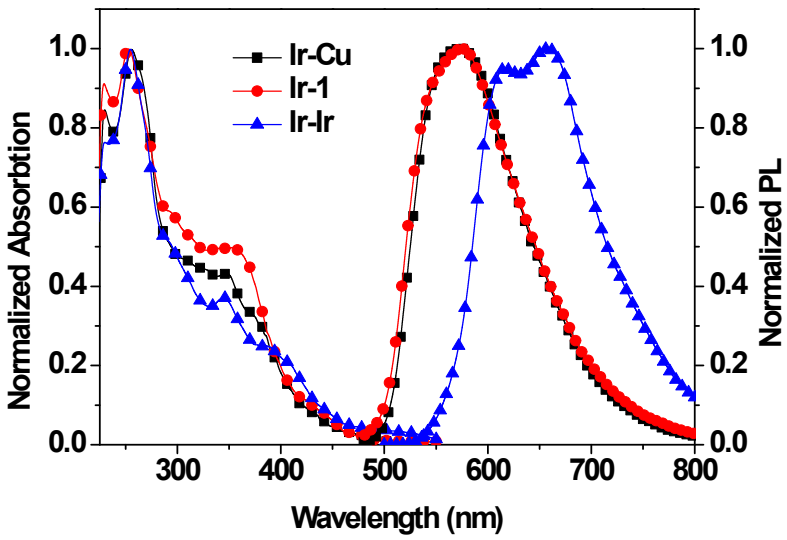

Fig. S4. UV absortion and PL spectrum of **Ir-Cu**, **Ir-1** and **Ir-Ir** in CH_2Cl_2 solution at room temperatures.

Table S2. Photophysical data comparision for **Ir-Cu**, **Ir-1** and **Ir-Ir**.

complex	λ_{abs}[a] nm (log ε)			PL[a] (nm)	Φ_{PL}[a] (%)	τ[a] (ns)
Ir-Cu	230(4.57), 294(4.44), 374(4.09), 450(3.16),	252(4.65), 304(4.45), 400(3.86), 500(2.63)	266(4.59), 338(4.37), 420(3.62),	575	21	1740
Ir-1	230(4.95), 290(4.79), 374(4.41), 450(3.41),	251(5.03), 304(4.80), 400(4.17), 500(2.84)	265(4.93), 339(4.71), 420(3.90),	574	29	512
Ir-Ir	230(4.54), 290(4.39), 374(4.04), 450(3.12),	251(4.61), 304(4.40), 400(3.82), 500(2.60)	265(4.52), 339(4.32), 420(3.57),	619,659	35	806

[a] Measured in degassed CH_2Cl_2 at a concentration of 10^{-4} M, and log ε values are shown in parentheses at 298 K. The excitation wavelength is 370 nm.

OLED Device characterization

The prepatterned indium tin oxide (ITO) substrates were cleaned by ultrasonic acetone bath, followed by ethanol bath. Afterwards, the substrates were dried with N_2 and then loaded into a UV-Ozone chamber. After UV-Ozone treatment, The PEDOT: PSS layer was spin-coated on the ITO substrate as the hole-injecting layer, and then annealed at 120 °C for 10 min inside the N_2-filled glove-box. The emitter layer was also prepared by spin-coating directly on the hole-injecting layer, and then annealed at 50 °C for 10 min. The electron-transporting material and the cathode material were thermally evaporated onto the emitter layer in a vacuum chamber. Before taken out of the glove-box, the devices were encapsulated with UV-curable epoxy. The voltage-current-luminance characteristics and the EL spectra were simultaneously measured with PR735 SpectraScan Photometer and Keithley 2400 sourcemeter unit under ambient atmosphere at room temperature.

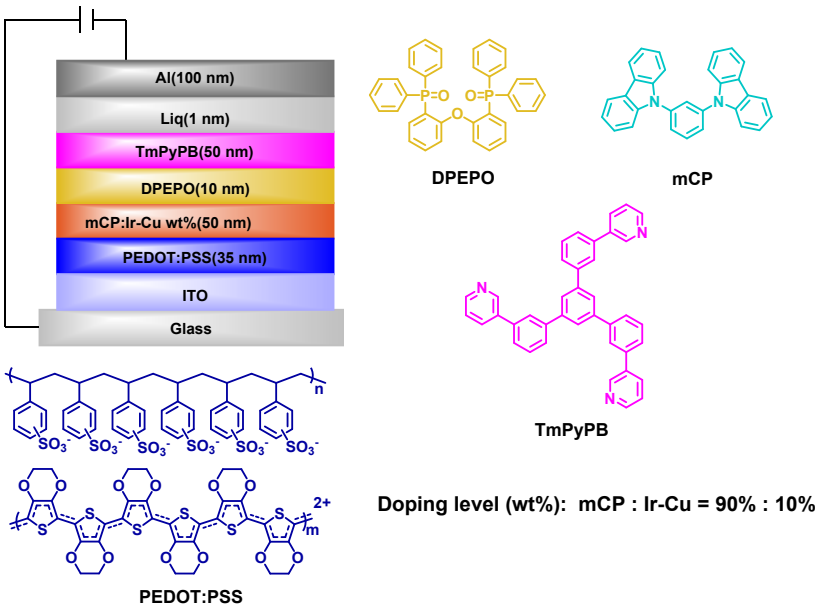

Fig. S5. Configuration of the OLEDs and chemical structures for the materials involved.

Table S3. EL performances of the device for **Ir-Cu**.

complex	V_{on}[a] [V]	$EQE_{max}/CE_{max}/PE_{max}$[b] [%/cd A^{-1}/lm W^{-1}]	λ_{ems}[c] [nm]	CIE[d] (x, y)
Ir-Cu	8	2.6/7.4/1.2	590	(0.49, 0.48)

[a] Voltage in the luminance of 10 cd/m^2. [b] Maximum external quantum efficiency (EQE_{max}), maximum current efficiency (CE_{max}), maximum power efficiency (PE_{max}). [c] Maximum emission wavelength of the EL spectra. [d] The Commission Internationale de I'Eclairage (CIE) coordinates.

DFT calculation

DFT method was used to optimize the geometries all the complexes. The electronic transition energies and electron correlation effects were also calculated by (TD)-DFT method with the B3LYP functional (TD-B3LYP). The LANL2DZ basis set was used to treat with the iridium atom and copper, and the 6–31G (d) basis set was used to treat with all other atoms. All calculations were carried out according to the Gaussian 09 program.[1]

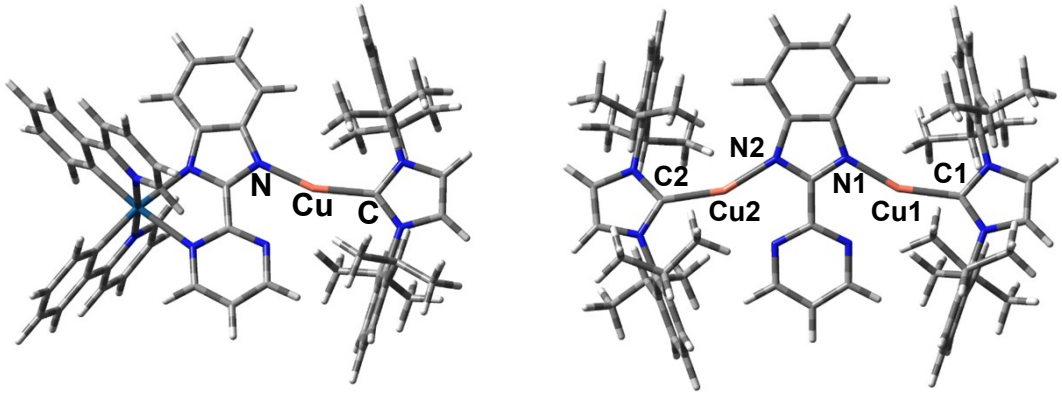

Ir-Cu

N-Cu-C:159.18°
Cu-C: 2.058Å
Cu-N: 1.991Å

Cu-Cu

N1-Cu1-C1:156.86°
Cu1-C1: 2.067Å
Cu1-N1: 1.997Å

N2-Cu2-C2:154.84°
Cu2-C2: 2.067Å
Cu2-N2: 1.997Å

Fig. S6. Calculated optimized structure for **Ir-Cu** and **Cu-Cu**.

Table S4. Calculated energies and oscillator strengths for lowest-energy singlet (S1) and triplet (T1) transitions.

complexes	states	E (eV)	Oscillator strength	main configurations (CI coeff)	Character
Ir-Cu	S_1	2.42	0.0001	HOMO→LUMO (0.65)	MLCT/LLCT
	T_1	2.32	0	HOMO-1→LUMO (0.57) HOMO→LUMO (0.36)	^{3}ILCT/^{3}MLCT/^{3}LLCT
Cu-Cu	S_1	2.90	0	HOMO-2→LUMO (0.70)	ILCT/MLCT
	T_1	2.58	0	HOMO→LUMO (0.67)	^{3}ILCT/^{3}MLCT

NMR spectra

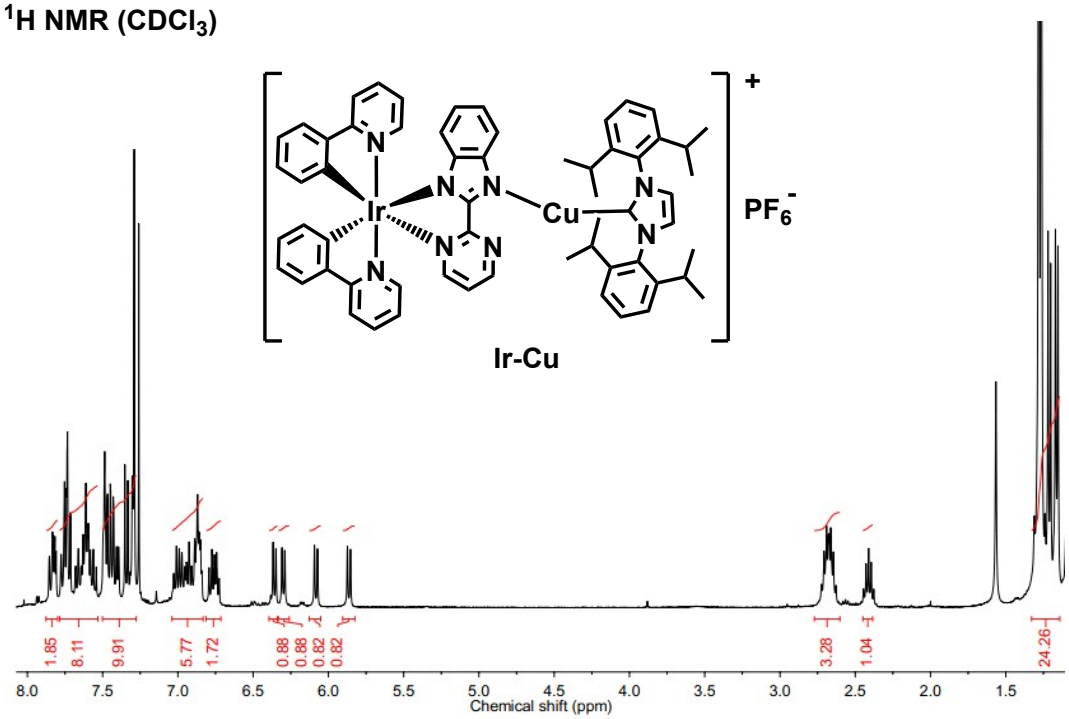

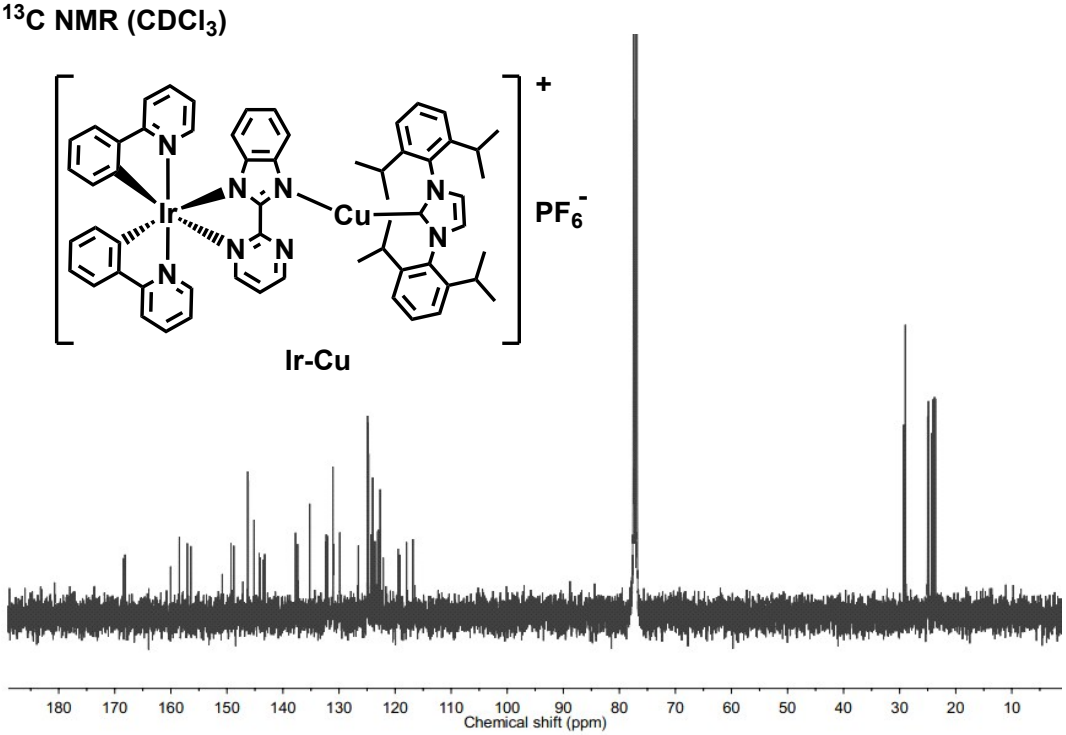

Fig. S7. ^{1}H NMR and ^{13}C NMR spectra of **Ir-Cu**.

^{1}H NMR ($CDCl_3$)

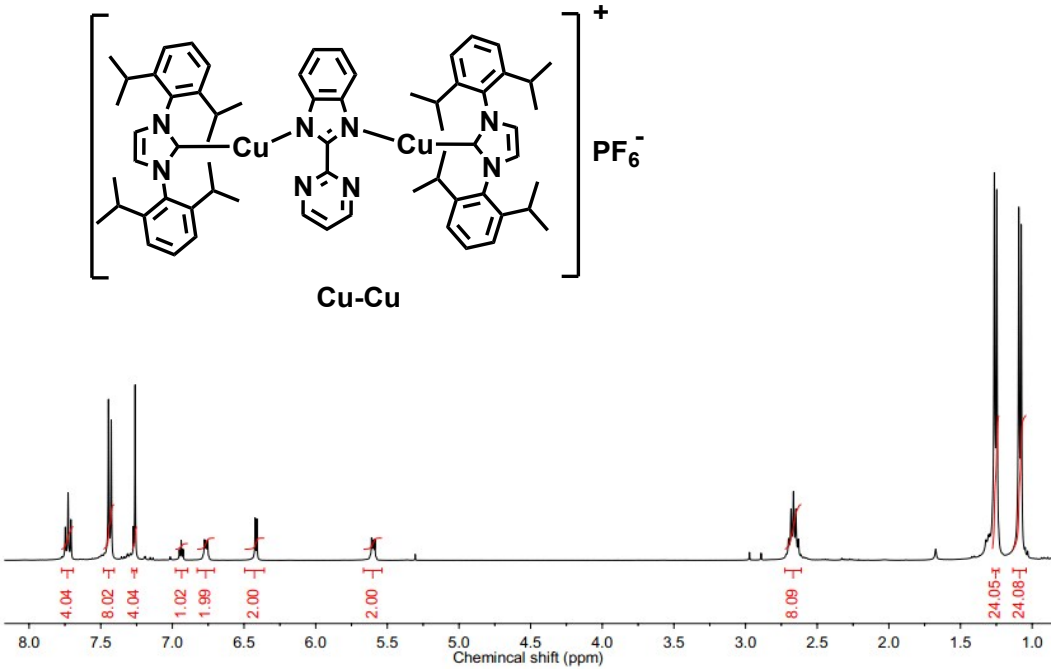

^{13}C NMR ($CDCl_3$)

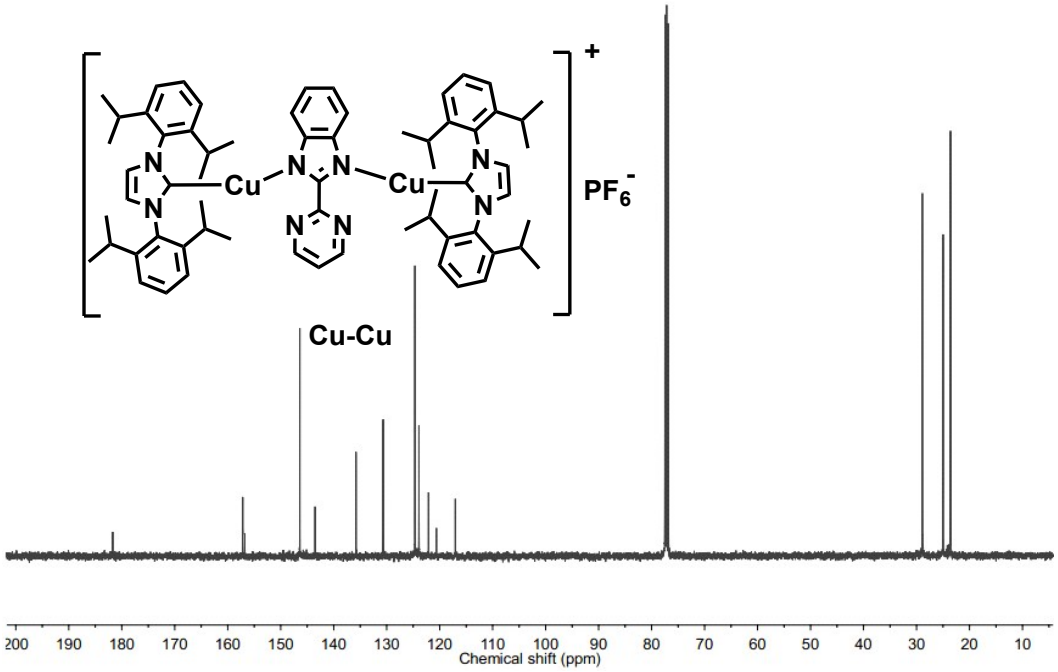

Fig. S8. ^{1}H NMR and ^{13}C NMR spectra of **Cu-Cu**.

References

1. M. J. Frisch, G. W. Trucks, H. B. Schlegel, G. E. Scuseria, M. A. Robb, J. R. Cheeseman, G. Scalmani, V. Barone, B. Mennucci, G. A. Petersson, H. Nakatsuji, M. Caricato, X. Li, H. P. Hratchian, A. F. Izmaylov, J. Bloino, G. Zheng, J. L. Sonnenberg, M. Hada, M. Ehara, K. Toyota, R. Fukuda, J. Hasegawa, M. Ishida, T. Nakajima, Y. Honda, O. Kitao, H. Nakai, T. Vreven, J. A. Montgomery Jr., J. E. Peralta, F. Ogliaro, M. Bearpark, J. J. Heyd, E. Brothers, K. N. Kudin, V. N. Staroverov, T. Keith, R. Kobayashi, J. Normand, K. Raghavachari, A. Rendell, J. C. Burant, S. S. Iyengar, J. Tomasi, M. Cossi, N. Rega, J. M. Millam, M. Klene, J. E. Knox, J. B. Cross, V.Bakken, C. Adamo, J. Jaram illo, R. Gomperts, R. E. Stratmann, O. Yazyev, A. J. Austin, R. Cammi, C. Pomelli, J. W. Ochterski, R. L. Martin, K. Morokuma, V. G. Zakrzewski, G. A. Voth, P. Salvador, J. J. Dannenberg, S. Dapprich, A. D. Daniels, O. Farkas, J. B. Foresman, J. V. Ortiz, J. Cioslowski and D. J. Fox, Gaussian 09, Revision B.01, Gaussian, Inc., Wallingford CT, **2010**.